Rate of runaway evaporative cooling

J. van de Groep, P. van der Straten,* and J. M. Vogels
Atom Optics and Ultrafast Dynamics, Utrecht University, P.O. Box 80,000, NL-3508 TA Utrecht, The Netherlands
(Received 27 May 2011; published 23 September 2011)

Evaporative cooling is a process that is essential in creating Bose-Einstein condensates in dilute atomic gasses. This process has often been simulated based on a model using a truncated Boltzmann distribution. This model assumes that the energy distribution up to the threshold energy can still be described by a Boltzmann distribution: it assumes detailed balance up to the threshold energy. However, the evolution of the distribution function in time is not taken into account. Here we solve the kinetic Boltzmann equation for a gas undergoing evaporative cooling in a harmonic and linear trap in order to determine the evolution of the energy distribution. The magnitude of the discrepancy with the truncated Boltzmannmodel is calculated by including a polynomial expansion of the distribution function. We find that up to 35% fewer particles are found in the high-energy tail of the distribution with respect to the truncated Boltzmann distribution and up to 15% more collisions are needed to reach quantum degeneracy. Supported by a detailed investigation of the particle loss rate at different energies, we conclude that the limited occupation of high-energy states during the evaporation process causes the lowering of the evaporation speed and efficiency.

DOI: 10.1103/PhysRevA.84.033628 PACS number(s): 67.85.−d, 37.10.De, 37.10.Gh

I. INTRODUCTION

Bose-Einstein condensation (BEC) can be obtained by cooling down a bosonic gas to an extremely low temperature, of the order of a few hundred nK [1–3]. The first part of the cooling of atoms at room temperature is in most cases performed by laser cooling which can cool down to typical ranges of mK [4]. The last part of the cooling process is performed by evaporative cooling.

Evaporative cooling is based on the selective removal of high-energy particles from a gas of atoms [5–7]. This can be summarized in two steps: the *evaporation* step, in which the particles with a total energy that is higher than a certain threshold energy ε_T are removed, and the *rethermalization* step, in which the kinetic energy is redistributed among the remaining particles using elastic collisions. The theory of evaporative cooling is complex and, so far, not fully understood. Although models are available describing the general characteristics of the cloud of atoms during the evaporation process [8,9], such as the temperature and the typical particle loss rate, the time evolution of the energy distribution is not fully described. These models are based on the assumption that the energy distribution is shaped as a truncated Boltzmann (tB) distribution up to the energy threshold and, thus, that detailed balance occurs up to the threshold energy. However, the validity of this assumption has, to our knowledge, never been verified.

Knowing the evolution of the energy distribution during evaporative cooling is of particular importance for an exciting new field of research: the realization of a continuous atom laser. The first atom lasers were created more than 10 years ago, where atoms are coupled out from a Bose-Einstein condensate to form a coherent atomic beam [10–13]. Since the condensate is depleted quickly, the outcoupling can only be continued after the creation of a new condensate and such an atom laser can only be considered a "pulsed" atom laser. A continuous atom laser can be achieved by cooling an atomic beam down to degeneracy, leading to a "truly" continuous beam of coherent atoms, which can be used for interferometry and atom optics [14]. Intensive research has been performed in this field [15–24]. To achieve a continuous atom laser, evaporative cooling is performed on a beam propagating through a magnetic guide. The time it takes to achieve degeneracy determines the required length of the magnetic guide. It is therefore important that the time evolution of the energy distribution is well understood.

The tB model is based on detailed balance between the elastic collisions taking place inside the cloud of atoms in order to reach thermalization. For the cloud of atoms to follow this distribution up to the threshold energy, detailed balance must therefore be fulfilled up to the threshold energy. Figure 1 shows why this condition is not fulfilled for all energies. In Fig. 1(a) particles 1 and 2, with energies below ε_T, collide, resulting in a high-energy particle (4) and a low-energy particle (3). The reverse process is possible and is equally probable, such that detailed balance is fulfilled. Figure 1(b) shows what happens with energies close to ε_T. Here one of the particles gains enough energy from the collision to exceed ε_T and to be evaporated. Therefore the reverse process is not possible and detailed balance is broken. This changes the dynamics of the evaporation process and slows it down.

The goal of this research is to accurately determine the evolution of the energy distribution in order to calculate the evaporation efficiency and the time it takes to reach quantum degeneracy. In order to determine the evolution of the energy distribution, the Boltzmann equation is solved. A polynomial expansion of the Boltzmann distribution for the energy of the atoms is used in order to take into account deviations from this distribution. Thus the actual energy distribution can be described accurately and is used to determine how long it takes for quantum degeneracy to occur. The calculation is performed for a monatomic gas in a harmonic and a linear magnetic trap but is applicable to any trapping potential. The method also provides the possibility to determine the

*p.vanderstraten@uu.nl

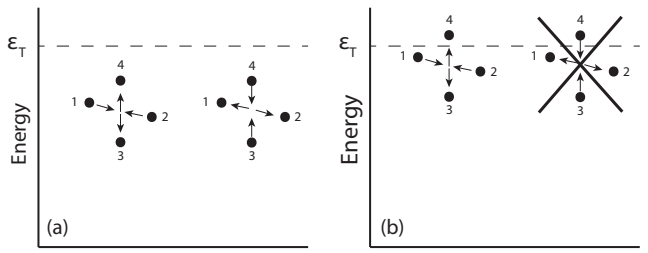

FIG. 1. Elastic collisions in energy space. Left: Detailed balance for particles with energies below the threshold energy ε_T, assuming a truncated Boltzmann model. Each collision process throughout the distribution function has equal probability of occurring in the opposite direction. Right: How detailed balance is broken near the threshold; the reverse process is not possible because particle 4 is evaporated, as indicated by the cross.

deviations quantitatively and to allow for evaporation schemes using a varying threshold energy.

II. THEORY

A. Evaporative cooling

As mentioned in the introduction, evaporative cooling is based on two steps. The first step is evaporating the high-energy particles. This can be done by using adjustable potential barriers that only capture particles with a total energy lower than a threshold energy ε_T. Removing the high-energy tail causes the distribution to be out of equilibrium. The second step is restoring equilibrium by redistributing the kinetic energy among the remaining particles by the use of elastic collisions. For simplicity, only elastic two-body s-wave collisions are included. Losses due to vacuum and three-body collisions are neglected. This simplifies the collision integral, which is discussed later. After this process—called rethermalization—the average energy per particle has been lowered, which results in a lower average temperature. We assume that all particles with an energy higher than ε_T are immediately evaporated. This is called full evaporation. For further cooling, the potential barriers can be lowered. In our calculations an evaporation scheme based on a constant evaporation parameter $\eta = \varepsilon_T/k_BT$ is used. This indicates that η is an indicator of the potential trap depth.

Experimentally, evaporative cooling is performed by using radio-frequency (rf) antennas to induce an rf transition from a trapped state into a nontrapped state [25]. This so-called "radio-frequency-induced evaporation" was first introduced by the Walraven group [26] and the Pritchard group [27]. For Rb and Na, typical evaporation schemes lower the rf from 60 to ~0.8 MHz in a time interval between 15 and 40 s [28].

One of the most important characteristics of evaporative cooling is the particle loss rate, which is determined by the evaporation scheme. Calculations on the particle loss rate usually focus only on the number of particles exceeding ε_T, since the tB model assumes detailed balance up to the energy threshold. However, as shown in Fig. 1, detailed balance breaks down near ε_T since the reverse process cannot occur. This results in a lower occupation of energy states just below ε_T. The tB model assumes the filling rate of these high-energy states—governed by collisions at lower energy that fulfill detailed balance—to be fast enough to maintain equilibrium up to the threshold. Therefore the detailed shape of the distribution below ε_T is often neglected in calculations. However, it is not clear whether this assumption is always fulfilled. During the refilling time the high-energy states are less occupied, causing a "hole" in the distribution function. The result is that the evaporation process is less likely to occur. This gives rise to the argument that the limited availability of high-energy states slows down the evaporation process. In our calculations, the particles with an energy lower than ε_T are included in order to find the actual shape of the distribution function and thereby to check the validity of the tB model.

B. Boltzmann equation

The time evolution of the evaporation process is described by the Boltzmann equation. The Boltzmann equation is used to describe the phase-space distribution $f(\mathbf{r},\mathbf{p})$ of a classical gas and the Boltzmann distribution is the solution, when no evaporation takes place. We assume that the gas can be treated classically, namely, that $n\Lambda^3 \ll 1$. Here, n is the density and $\Lambda = h/\sqrt{2\pi m k_B T}$ is the deBroglie wavelength. This assumption is valid for most of the evaporation time. The advantage of this assumption is that the Boltzmann statistics can be used instead of the Bose-Einstein statistics and that we can use the Boltzmann equation to determine the evolution of the energy distribution.

The Boltzmann equation is given by

$$\left(\frac{\mathbf{p}}{m}\cdot\nabla_r - \nabla_r U\cdot\nabla_p + \frac{\partial}{\partial t}\right) f(\mathbf{r},\mathbf{p}) = \Im(\mathbf{r},\mathbf{p}), \tag{1}$$

with the collision integral $\Im$ given by

$$\Im(\mathbf{r},\mathbf{p}) = \frac{\sigma}{(2\pi\hbar)^3 2\pi m}\iint |\mathbf{p}_{\rm rel}|\delta(\mathbf{p}_3+\mathbf{p}_4-\mathbf{p}_2-\mathbf{p}) \times[f(\mathbf{r},\mathbf{p}_3)f(\mathbf{r},\mathbf{p}_4) - f(\mathbf{r},\mathbf{p}_2)f(\mathbf{r},\mathbf{p})]d\mathbf{p}_2 d\mathbf{p}_3 d\mathbf{p}_4 d\Omega. \tag{2}$$

Here, U is the trapping potential, m is the mass of the particles, ∇_r is the spatial gradient, and ∇_p is the momentum gradient. The collision integral $\Im(\mathbf{r},\mathbf{p})$ on the right side of the equation describes the effects of the various collisions on the atoms with momentum $\mathbf{p}$. Furthermore, $\mathbf{p}$ and $\mathbf{p}_2$ are the momenta of the two colliding atoms before the collision, and $\mathbf{p}_3$ and $\mathbf{p}_4$ after the collision, σ is the collisional cross section, and Ω is the collision angle. The first term in brackets on the right side of Eq. (2) represents the "production" process of particles with momentum $\mathbf{p}$, and the second term the "destruction" process. Note that our model does not allow for inelastic losses, which, for certain systems, may be important. However, in the comparison between the tB model and our model these losses contribute to both models equally and thus do not change the conclusions from our analysis.

III. METHOD

A. Building the Boltzmann equation

To determine the time evolution of the distribution function the Boltzmann equation of Eq. (1) must be solved. This can be done analytically by using a Boltzmann distribution with

a polynomial expansion and an energy-dependent approach, which is based on the work of Luiten *et al.* [9]. They use the density of states and the energy-dependent distribution function instead of the momentum-dependent distribution function. To convert from the momentum- to the energy-dependent distribution function, we assume that the distribution of the particles in phase space depends only on their energy. This is referred to as "sufficient ergodicity" and it greatly simplifies the calculations [9]. This assumption is valid if the trap frequencies are much higher than the mean collision rate. An advantage of this approach is that it can be used for different trapping potentials, since only the density of states $\rho(\varepsilon)$ depends on the external trapping potential. Using the assumption of sufficient ergodicity the density of states is given by [9]:

$$\rho(\varepsilon) = (2\pi\hbar)^{-3} \iint \delta\left(\varepsilon - U(\mathbf{r}) - \frac{p^2}{2m}\right) d\mathbf{r}d\mathbf{p}. \tag{3}$$

Here, the Dirac δ function ensures energy conservation. Evaluating the momentum integral yields

$$\rho(\varepsilon) = \frac{2\pi(2m)^{3/2}}{(2\pi\hbar)^3} \int_{U(\mathbf{r})\leqslant\varepsilon} \sqrt{\varepsilon - U(\mathbf{r})} d\mathbf{r}. \tag{4}$$

The density of states can be calculated by inserting the specific external trapping potential $U(\mathbf{r})$ and integrating over space.

The assumption of ergodicity simplifies the Boltzmann equation since the system can be treated locally homogeneous [9]. It allows the distribution function to be written in terms of energy:

$$f(\mathbf{r},\mathbf{p}) = \int \delta\left(U(\mathbf{r}) + \frac{p^2}{2m} - \varepsilon\right) f(\varepsilon) d\varepsilon. \tag{5}$$

The result is that all terms of the Boltzmann equation drop out except for the time derivative of the distribution function. Combined with Eq. (3), the Boltzmann equation can be written as [9]

$$\rho(\varepsilon)\frac{\partial f(\varepsilon)}{\partial t} = \frac{m\sigma}{\pi^2\hbar^3} \iint \delta(\varepsilon_3 + \varepsilon_4 - \varepsilon_2 - \varepsilon)\rho(\min(\varepsilon,\varepsilon_2,\varepsilon_3,\varepsilon_4)) \times [f(\varepsilon_3)f(\varepsilon_4) - f(\varepsilon_2)f(\varepsilon)] d\varepsilon_2 d\varepsilon_3 d\varepsilon_4, \tag{6}$$

where ε_i is the energy of particle i ($i = 2,4$):

$$\varepsilon_i = \frac{p_i 2}{2m} + U(\mathbf{r}). \tag{7}$$

This equation can be used to calculate the time evolution of the distribution function and is referred to as the (kinetic) Boltzmann equation. Note that this equation monitors the time evolution of the energy state occupied by a particle with energy ε and that it can be used for different trapping potentials. Instead of numerical integration to solve the Boltzmann equation [9], we use a polynomial expansion of the distribution function to calculate the time evolution.

To calculate the actual shape of the distribution function during the evaporation process, the distribution function is extended with a polynomial expansion. The polynomial expansion will correct for the deviations from the tB model and will thus be a direct measure of discrepancies. The discrepancies are expected to be a function of energy since detailed balance breaks down close to ε_T. Therefore, the polynomial expansion consists of various orders of ε:

$$f(\varepsilon,t) = \begin{cases} NAP(\varepsilon)e^{-\varepsilon/k_BT}, & \varepsilon < \varepsilon_T, \\ 0, & \varepsilon > \varepsilon_T, \end{cases} \tag{8}$$

with

$$P(\varepsilon) = 1 + \sum_{i=2}^{\infty} p_i \left(\frac{\varepsilon}{k_BT}\right)^i. \tag{9}$$

Here, A is a normalization constant that depends on the trapping potential due to the normalization condition $\int_0^\infty \rho(\varepsilon) f(\varepsilon,t) d\varepsilon = N$. Note that the normalization is performed without the polynomial expansion [$P(\varepsilon) \equiv 1$], so that A does not depend on p_i. The dimensionless constants p_i are time dependent, but we show that under certain conditions they are constant. Furthermore, $f(\varepsilon > \varepsilon_T,t) = 0$ due to the evaporation knife at $\varepsilon = \varepsilon_T$. Note that the equilibrium Boltzmann distribution can be obtained by setting $p_i = 0$ and $\varepsilon_T = \infty$. The polynomial expansion is determined by p_i that need to be determined. Since a distribution function is mainly characterized by the density and the temperature, two degrees of freedom should be eliminated by setting $p_0 \equiv 1$ for the zeroth order and $p_1 \equiv 0$ for the first order (ε^1). This guarantees that the system is not under-determined. The polynomial expansion is expanded at least up to the fourth order in ε.

B. Time-independent scaling

The purpose of the model is to determine how long it takes to reach quantum degeneracy. This can be done by monitoring the evolution of the collision rate, density, and temperature. However, we can exploit the behavior of the distribution function throughout the evaporation process to scale out the time dependence. As described below, during the evaporation process the distribution function is characterized by self-similarity. The distribution function will be cast through the thermalization process into a shape that is identical for all times. Although the particles individually continuously change their energy and thereby their location inside the distribution function, the overall shape will remain the same. For instance, by introducing the reduced energy ε_i/k_BT the collision integral on the right side of Eq. (6) is scaled in such a way that it becomes time-independent.

Our analysis starts with the notion that the rate of the evaporation process is determined by the number of collisions. After a finite number of collisions all relevant quantities for the evaporation process have increased or decreased with a certain fraction. For the collision rate γ this means that the time derivative depends quadratically on γ, since if the rate increases, not only does γ increase, but also the time decreases, in which the number of collisions takes place. Thus $d\gamma/dt = \alpha\gamma^2$, with α a proportionality constant. Its solution is $\gamma = \gamma_0(1 - t/t_0)^{-1}$, where t_0 is a constant determining the time scale of the process, $\gamma_0 = \langle n_0\rangle\sigma\langle v_{\rm rel}\rangle$ is the initial mean collision rate, $\langle n_0\rangle$ is the initial average density, and $\langle v_{\rm rel}\rangle = \sqrt{16k_BT_0/\pi m}$ is the average relative velocity between two colliding particles. In a similar way we can express the time dependence of the temperature T and number of particles N as [29]

$$T(t) = T_0\left(1 - \frac{t}{t_0}\right)^{\alpha_T}, \quad N(t) = N_0\left(1 - \frac{t}{t_0}\right)^{\alpha_N}, \tag{10}$$

where T_0 and N_0 are the initial temperature and number of particles, respectively, and α_T and α_N are constants that need to be determined. Note that Eqs. (10) show the typical time behavior for runaway evaporative cooling, where the temperature and number of particles progressively go to 0 for t approaching t_0. Since both parameters change over many orders of magnitude during the evaporation process and degeneracy is reached close to this point, we use t_0 in our model as the time it takes to reach degeneracy. Clearly, for $t_0 > 0$ the collision rate in our model asymptotically goes to infinity at t_0, and in that case degeneracy is always reached just before t_0, whatever the initial conditions are for the temperature and the number of particles.

Using the reduced energy ε_i/k_BT and Eqs. (10) for $N(t)$ and $T(t)$, both sides of the kinetic Boltzmann equation have the same time dependence, if α_N is given by

$$\alpha_N = \alpha_T\left(\delta - \tfrac{1}{2}\right) - 1, \tag{11}$$

where $\delta = 3/s$ is the exponent of the potential $V = \lambda r^s$. For a harmonic trap $\delta = 3/2$ and $\alpha_N = \alpha_T - 1$, whereas for a linear trap $\delta = 3$ and $\alpha_N = 5\alpha_T/2 - 1$.

The Boltzmann equation is made dimensionless by introducing the critical number of collisions N_c, which is defined as

$$N_c \equiv \gamma_0 t_0 = \langle n_0\rangle\sigma\sqrt{\frac{16k_BT}{\pi m}}t_0. \tag{12}$$

Here γ_0 is calculated at $t = 0$ using the untruncated Boltzmann distribution function and $\langle n_0\rangle$ is the average density in the trap at $t = 0$. The resulting Boltzmann equation is both time independent and dimensionless. The solution determines the distribution function irrespective of the temperature and/or time, and thus the values of p_i are time independent. This is the direct proof that the energy distribution function has become self-similar. Note that N_c is the number of collisions that will take place between $t = 0$ and $t = t_0$, in case the evaporation process does *not* change the collision rate. However, in our model the collision rate increases as a function of time, and in fact the number of collisions between $t = 0$ and $t = t_0$ in our model becomes infinite. The critical number of collisions N_c is the crucial parameter to be determined in our model.

C. Solving the Boltzmann equation

Using the method in Sec. III B the variables of interest are N_c, α_T, and p_i. In order to solve for these variables, the *method of moments* is used. This method "projects" the kinetic Boltzmann equation onto functions of energy $\Psi(\varepsilon) = 1, \varepsilon, \varepsilon^2, \ldots$ and is integrated over energy to obtain the moment equations. The zeroth order corresponds to the conservation of particles, and the first order to the conservation of energy. Using this method, sufficient equations are generated to obtain a closed system of equations. If the polynomial expansion is extended with an extra term, only the next order moment needs to be included. Note that if $P(\varepsilon) = 1$, we have detailed balance up to ε_T and obtain the tB model. In that case only N_c and α_T are unknown and the conservation of particles and energy provides sufficient information.

The method of moments can only be used if the integrals over energy space can be performed. The left side of the Boltzmann equation is linear in $f(\varepsilon)$ and thus in p_i. The right side of Eq. (6) is bilinear in p_i since it consists of two linear terms. The integrals over the distribution functions can be done independently and analytically, leading to the moment equations for p_i.

Evaluating the integrals in Eq. (6) is complicated due to the fact that the limits of integration are related to each other. Also, the right side of the Boltzmann equation uses the minimum energy of all four particles to determine the density of states and the integration area needs to be divided into separate regions with different limits. First, we replace $\varepsilon_2 = \varepsilon_3 + \varepsilon_4 - \varepsilon$ on the right side of Eq. (6) due to energy conservation. Next, we integrate over ε_4 and ε_3, where the limits depend on ε. Finally, we integrate ε over the entire range of $0 \leqslant \varepsilon \leqslant \varepsilon_T$. The limits of the regions with different minimum energies can be determined using the condition that all energies must be higher than 0.

The different regions and their limits are determined using Fig. 2. After combining the regions with equal minimum energies, four regions remain. Since in each region we have a production term $[f(\varepsilon_3)\cdot f(\varepsilon_4)]$ and a destruction term $[f(\varepsilon_2)\cdot f(\varepsilon)]$, we end up with eight integrals. Finally, one of these must be split up into two separate regions (integrals 6 and 7) in order to ascertain that $\varepsilon_2 = \varepsilon_3 + \varepsilon_4 - \varepsilon$, given the order in which the integration over ε_4 and ε_3 is performed. This yields nine integrals that can now be solved analytically. A summary of all integrals, the distribution functions involved, the local minimum energy, and the limits of integration is reported in Table I.

After performing the integrals there are various parameters in the equations such as σ, T_0, N_0, and parameters characterizing the trap. However, the only relevant parameter in the scaled Boltzmann equation is N_c, which only depends on η and is thus independent of these parameters. However, t_0 is

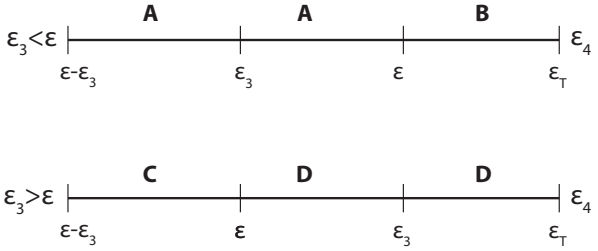

Range	ε_{min}
A	ε_2
B	ε_3
C	ε_4
D	ε

FIG. 2. The different regions for integration expressed in terms of ε_4. Lines represent ε_4 increasing from $\varepsilon - \varepsilon_3$ to ε_T for two conditions of ε_3. The letters A–D represent the minimum energy in that region.

TABLE I. Limits for integration and the minimum energy for each integral. The range for ε is in each integral $[0,\varepsilon_T]$.

Integral	Functions involved	Minimum energy	Range	
			ε_3	ε_4
1	$f(\varepsilon_3)f(\varepsilon_4)$	ε_2	$[0,\varepsilon]$	$[\varepsilon-\varepsilon_3,\varepsilon]$
2	$f(\varepsilon_2)f(\varepsilon)$	ε_2	$[0,\varepsilon]$	$[\varepsilon-\varepsilon_3,\varepsilon]$
3	$f(\varepsilon_3)f(\varepsilon_4)$	ε_3	$[0,\varepsilon]$	$[\varepsilon,\varepsilon_T]$
4	$f(\varepsilon_2)f(\varepsilon)$	ε_3	$[0,\varepsilon]$	$[\varepsilon,\varepsilon+\varepsilon_T-\varepsilon_3]$
5	$f(\varepsilon_3)f(\varepsilon_4)$	ε_4	$[\varepsilon,\varepsilon_T]$	$[0,\varepsilon]$
6	$f(\varepsilon_2)f(\varepsilon)$	ε_4	$[\varepsilon,\varepsilon_T]$	$[0,\varepsilon]$
7	$f(\varepsilon_2)f(\varepsilon)$	ε_4	$[\varepsilon_T,\varepsilon_T+\varepsilon]$	$[0,\varepsilon_T-\varepsilon_3+\varepsilon]$
8	$f(\varepsilon_3)f(\varepsilon_4)$	ε	$[\varepsilon,\varepsilon_T]$	$[\varepsilon,\varepsilon_T]$
9	$f(\varepsilon_2)f(\varepsilon)$	ε	$[\varepsilon,\varepsilon_T]$	$[\varepsilon,\varepsilon_T-\varepsilon_3+\varepsilon]$

TABLE II. Parameters defining the harmonic and linear potential trap. Here ω is given by the geometrical mean of the different trap dimensions: $\omega=(\omega_x\omega_y\omega_z)^{1/3}$. A is calculated using $P(\varepsilon)=1$ and $\varepsilon_T=\infty$.

Property	Harmonic trap	Linear trap
Trap potential $U(r)$	$\frac{1}{2}m\omega^2r^2$	λr
Density of states $\rho(\varepsilon)$	$\frac{\varepsilon^2}{2(\hbar\omega)^3}$	$\frac{32\sqrt{2}}{105\pi}\frac{\varepsilon^{7/2}}{(\hbar^2\lambda^2/m)^{3/2}}$
Norm. constant A	$\left(\frac{\hbar\omega}{k_BT}\right)^3$	$\left(\frac{\pi^{1/3}\hbar^2\lambda^2}{2mk_B^3T^3}\right)^{3/2}$
Average density $\langle n_0\rangle$	$\frac{N}{8}\left(\frac{m\omega^2}{\pi k_BT_0}\right)^{3/2}$	$\frac{N}{\pi}\left(\frac{\lambda}{4k_BT_0}\right)^3$
Collision rate γ_0	$\frac{N\sigma m\omega^3}{2\pi^2k_BT_0}$	$\frac{N\sigma\lambda^3}{16\sqrt{\pi^3m(k_BT_0)^5}}$
Energy per particle E	$3nk_BT$	$\frac{9}{2}nk_BT$
Evap. efficiency η_{eff}	$\frac{6\alpha_T-3}{\alpha_T-1}$	$\frac{63\alpha_T-18}{10\alpha_T-4}$

determined by Eq. (12) and therefore does depend on these parameters. This indicates that the critical number of collisions N_c is constant: only the time it takes for these collisions to take place is determined by the initial conditions and the trap. The critical number of collisions N_c is thus independent of the initial phase space density. Note that if $t_0<0$, the exponents of the density and temperature also switch sign ($\alpha_T<0$, $\alpha_N<0$). Under these conditions the evaporation is no longer runaway and the temperature still decreases, but the collision rate also decreases and $T=0$ will never be reached.

The results obtained from the Boltzmann equation show the dependence of N_c on the evaporation parameter η and are used to determine the most efficient evaporation parameter, for which N_c is at a minimum. However, η represents the location of the evaporation knife, thereby reflecting the lower bound of energy that is evaporated by cutting away the high-energy particles. Since including the polynomial expansion changes the energy distribution of the particles, this also changes the average energy per evaporated particle. We therefore introduce the effective evaporation efficiency η_{eff}, which reflects the effective amount of energy that is removed per evaporated particle:

$$k_BT\eta_{\text{eff}}\equiv\frac{dE}{dN}=\frac{dE/dt}{dN/dt}. \tag{13}$$

Since the amount of energy removed per particle is higher than η, it shows that η_{eff} rather than η describes the evaporation efficiency. Furthermore, Eq. (13) allows us to write η_{eff} in terms of α_T, as reported in Table II.

The method to solve the Boltzmann equation has now been described. In Sec. IV we apply this method to both a harmonic and a linear potential trap. For both traps the effect of the polynomial expansion is calculated together with N_c as a function of η and η_{eff}. These calculations are performed by substituting the potential in Eq. (4) and using the result to find A, the average density $\langle n\rangle$, N_c, and η_{eff}. The effective efficiency η_{eff} is obtained by inserting Eq. (10) in Eq. (13) and applying the product rule for the derivatives. The trap-dependent parameters are summarized in Table II.

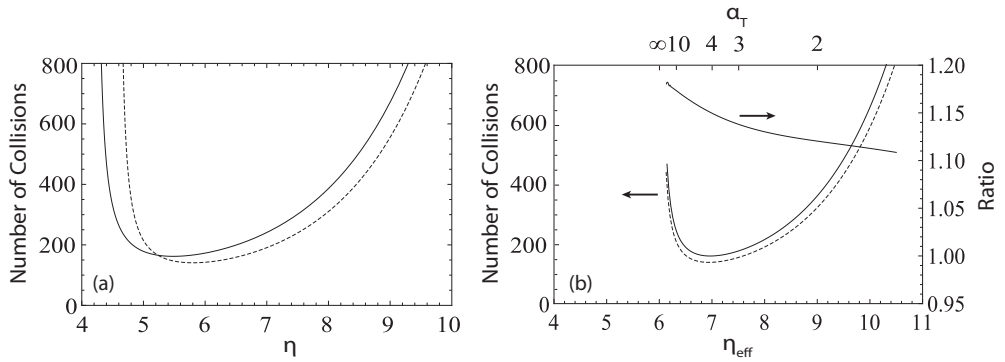

FIG. 3. (a) The critical number of collisions N_c as a function of η for our model (solid line) and the tB model (dashed line) for a harmonic trap. The horizontal shift of the two lines with respect to each other is a result of the difference in the average energy per evaporated particle. (b) The critical number of collisions N_c (scale on the left) as a function of η_{eff} for our model (solid line) and the tB model (dashed line). The corresponding values of α_T are shown at the top of the graph. The ratio (scale on the right) between our model and the tB model exceeds 1 over the entire range of η_{eff}.

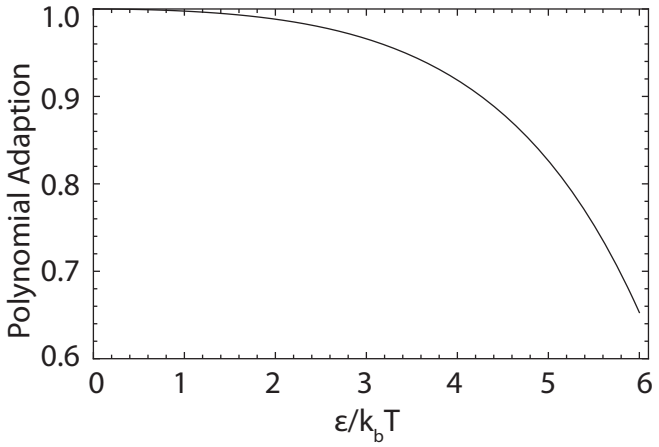

FIG. 4. Effect of polynomial expansion $P(\varepsilon)$ on the distribution function for $\eta = 6$. The discrepancy increases with energy up to 35% at the evaporation knife located at $\varepsilon/k_BT = 6$.

IV. RESULTS AND DISCUSSION

Here we discuss the results for the harmonic trap, followed in Sec. IV B by the results for the linear trap.

A. Harmonic trap

The distribution function in Eq. (8) is used to calculate N_c as a function of η, as shown in Fig. 3(a). The results are obtained by expanding the polynomial expansion up to the sixth order and compared with the tB model. From Fig. 3(a), one observes that in our model the minimum of N_c is 162.1 for $\eta = 5.48$, whereas for the tB model the minimum of N_c is 140.8 for $\eta = 5.8$. Thus N_c calculated using the tB model is 15.1% lower and the corresponding value for η is higher. A better comparison is made when N_c is plotted as a function of η_{eff} [Eq. (13)], as shown in Fig. 3(b). We observe that the minimum of N_c now occurs at the same η_{eff} for both models and that the tB model underestimates N_c over the entire range of η_{eff}. The discrepancy at the minimum of N_c is 15.1% and is more than 10% over the entire range. Figure 3 shows that the evaporation process is most efficient when $\eta \approx 6$.

The discrepancy of the distribution from the tB model can be calculated directly by the use of the polynomial expansion. In Fig. 4 the effect of the polynomial expansion (expanded up to p_6) as a function of energy is shown for $\eta = 6$. This figure clearly shows that there are up to 35% fewer particles in the high-energy range of the distribution than assumed in the tB model. The calculation not only shows that there is a large discrepancy, but also directly indicates the origin of the reduced evaporation efficiency.

The difference between the distribution function in our model and that in the tB model can be further investigated by determining the particle loss rate. The zeroth-order moment equation corresponds to the conservation of particles. This equation is obtained by projecting both sides of the Boltzmann equation (6) onto $\Psi(\varepsilon) = 1$ and integrating over energy. However, by determining the integrands of both sides one obtains insight into the particle loss rate at different energies. Figure 5(a) shows the particle loss rate as a function of energy calculated using the tB model for $\eta = 6$. The solid line corresponds to the left side of the Boltzmann equation and represents the time evolution of the distribution function. The dashed line corresponds to the right side of the Boltzmann equation and refers to the collision integral. Note that integration of both curves over ε yields the total particle loss rate and they are therefore equal. The general trend of both curves indicates how the evaporation process works: negative values at high energies (high-energy particles are evaporated) and positive values at low energies (low-energy particles are formed through rethermalization). However, Fig. 5(a) shows that the tB model fails to describe the evaporation process in detail: the curves do not overlap. The negative value in the residual error around $\varepsilon/k_BT \sim 3$ indicates that the tB model underestimates the particle loss rate at this energy. Furthermore, the positive values near the threshold energy ($\varepsilon/k_BT \sim 6$) indicate that the model overestimates the evaporation of high-energy particles. This means that the tB model overestimates the evaporation efficiency and therefore underestimates N_c. This is consistent with the results in Fig. 4, since there are fewer particles in the high-energy tail of the distribution and the loss rate of these particles is also lower.

The results for our model are shown in Fig. 5(b). The two lines almost completely overlap and the residual error is reduced by 4 orders of magnitude compared to the tB model. The small error indicates that the results are nearly converged. The results show that the polynomial expansion in our model

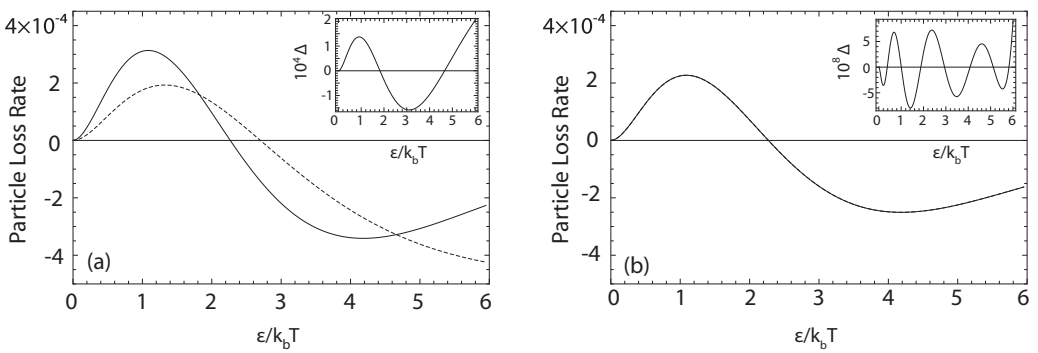

FIG. 5. (a) Particle loss rate as a function of energy obtained by projecting the left side (solid line) and right side (dashed line) of the Boltzmann equation on $\Psi = 1$ using the tB model for a harmonic trap. Inset: Residual error Δ as a function of energy. (b) Particle loss rate as a function of energy using our model. The two lines almost completely overlap and the inset shows that the residual error Δ is as small as $\sim 10^{-8}$.

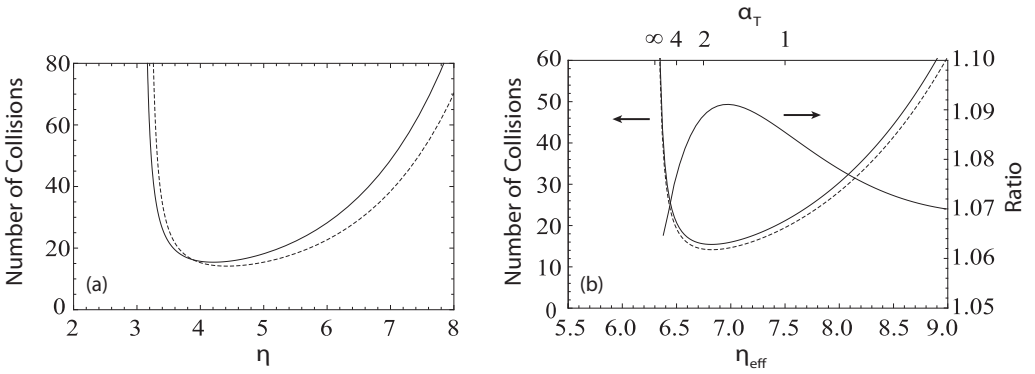

FIG. 6. (a) Critical number of collisions N_c as a function of η calculated for our model (solid line) and the tB model (dashed line) for a linear trap. (b) Critical number of collisions N_c (scale on the left) as a function of η_{eff} calculated with our model (solid line) and the tB model (dashed line). The corresponding values of α_T are shown at the top of the graph. The ratio (scale on the right) between the two models exceeds 1 over the entire range.

is able to describe the evolution of the distribution function in detail and that the results calculated using our model are reliable.

B. Comparing linear trap with harmonic trap

The shape of the trap influences the evaporation process by changing the spatial particle distribution in the trap. The results for the linear trap are discussed in comparison with the results for the harmonic trap.

In Fig. 6(a), N_c is shown as a function of η. A trend similar to that in Fig. 3 is observed: the minimum in our model lies higher than that in the tB model and is shifted horizontally. A detailed comparison shows three issues: (1) N_c is smaller compared to the harmonic trap (20, compared to 140), (2) the corresponding value for η is lower (4.3, compared to 5.5), and (3) the difference between the two lines is smaller (9%, compared to 15.1% for the harmonic trap). The difference in N_c can be attributed to the stronger confinement of the linear trap with respect to the harmonic trap. In Fig. 6(b) N_c is plotted as a function of η_{eff}. As for the harmonic trap the figure shows that the tB model always underestimates N_c. The discrepancy is smaller than for the harmonic trap but is always larger than 6%.

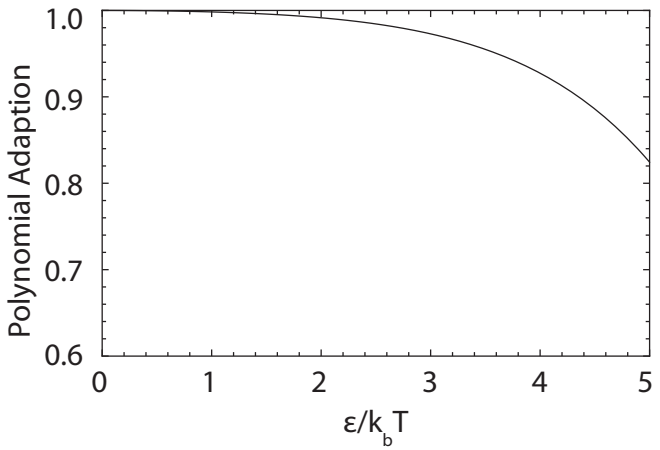

FIG. 7. Effect of polynomial expansion $P(\varepsilon)$ on the distribution function for $\eta = 5$. The evaporation knife is located at $\varepsilon/k_BT = 5$.

The discrepancy from the tB model as shown in Fig. 7 shows a similar trend as for the harmonic trap, although the discrepancies are smaller. The discrepancy increases with energy up to 17.6% at the threshold, compared to 35% for the harmonic trap. This indicates that primarily the high-energy states within the distribution are less occupied than determined by the tB model.

The particle loss rate as a function of energy is used to investigate the origin of the discrepancies, as discussed in Sec. IV A. Figure 8(a) shows the results for the tB model, and Fig. 8(b) the results for our model. Comparing Fig. 8(a) to the harmonic case [Fig. 5(a)] shows that although the residual error is 1 order of magnitude smaller ($\sim 10^{-5}$), the trend is identical. The tB model overestimates the evaporation rate of high-energy particles near the threshold energy and underestimates the loss rate of particles with energies around $\varepsilon/k_BT \sim 3.5$. The smaller residual error directly explains the smaller discrepancies with respect to the harmonic trap, as shown in Figs. 6(a) and 7. Figure 8(b) shows a result similar to that for the harmonic trap in Fig. 5(b): in our model both lines almost completely overlap, indicating that the collision integral is modeled accurately to reduce the residual error by 3 orders of magnitude.

C. Discussion

The results for the harmonic and linear trap show that the discrepancy of the time evolution of the distribution function in the tB model is present for different trapping potentials. Furthermore, the origin of the discrepancies is similar in both cases, as determined by the particle loss rates for different energies. The magnitude of the discrepancy is reduced in the case of the linear trap with respect to the harmonic trap. The results thus clearly show that the tB model does not describe the evaporation process accurately. For both the harmonic and the linear trap a discrepancy is found for the distribution, which increases with energy as shown in Figs. 4 and 7, respectively.

The discrepancies between the two models that we find are significant and it is surprising that these discrepancies did not show up in the work of Luiten *et al.* [9]. We attribute the differences mainly to the rapidly changing value for η in their

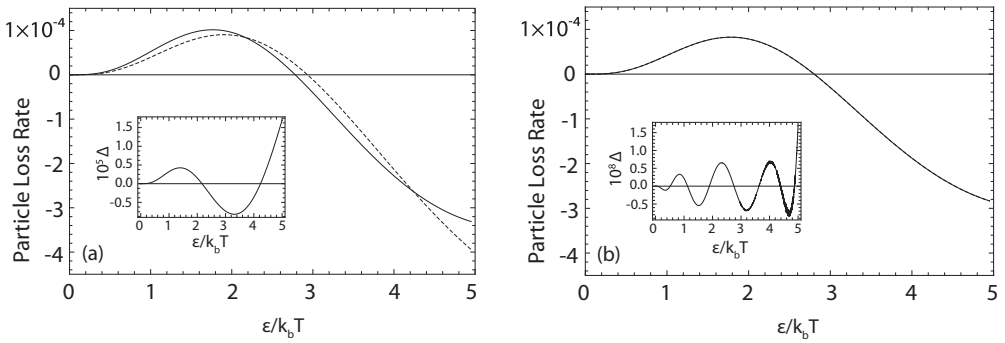

FIG. 8. (a) Particle loss rate as a function of energy obtained by projecting the left side (solid line) and right side (dashed line) of the Boltzmann equation on $\Psi = 1$ using the tB model for a linear trap. Inset: Residual error Δ as a function of energy. (b) Particle loss rate as a function of energy using our model. The two lines almost completely overlap and the inset shows that the residual error Δ is as small as $\sim 10^{-8}$.

work, due to which specific differences did not have enough time to establish. Specifically, discrepancies at low η might partially cancel discrepancies at high η.

Our formalism is easily extendable to allow for time-dependent η by allowing explicit time dependencies of A, p_i, and η. This allows simulation of the same physical situation as the simulation in Ref. [9]. Such a detailed comparison is beyond the scope of this paper. Moreover, our formalism allows for a correct description of the spilling process, including the reduction by depletion of high-energy states.

This model is based on several important assumptions. The assumption of sufficient ergodicity may, for example, not always be fulfilled. In the case of a cylindrical or spherical trap, not all particles with an energy above ε_T will be evaporated, thereby reducing the efficiency. Even in the tB approach this can lead to large discrepancies, for example, in one-dimensional cooling [29]. In future research we focus on an extended model that does not rely on these assumptions and includes different trapping potentials.

Finally, the results have implications for experiments implementing evaporative cooling on a propagating beam [18]. Due to a lower evaporation efficiency than expected based on the tB model, the magnetic guide needs to be 10%–15% longer in order to reach degeneracy, depending on the trapping potential that is used. Furthermore, these results will have no direct consequence for BEC experiments using trapped samples. The small increase in time that is needed to obtain BEC can simply be accounted for in the evaporation scheme.

V. CONCLUSION

We solve the Boltzmann equation to find the number of collisions required to reach runaway evaporative cooling and degeneracy. For both a harmonic and a linear trapping potential it is found that the high-energy states of the distribution function are less occupied during the evaporation process as assumed in the tB model. This lower occupation is caused by the fact that the refilling rate of these high-energy states is slow, resulting in a "hole" in the distribution function. Due to this hole the evaporation process is less likely to occur and thereby its efficiency is lowered. This is confirmed by an increase in the calculated number of collisions needed to reach BEC. Also, detailed investigation of the particle loss rate shows how the tB model overestimates the evaporation efficiency. We find that a reduction of particles in high-energy states with respect to the tB distribution is a limiting factor for evaporative cooling leading to a decrease in the evaporation efficiency. It can therefore be concluded that the evaporation efficiency is lower than expected based on the tB model due to the low occupancy of the high-energy states.

ACKNOWLEDGMENTS

This work is part of the VIDI research program on the Atom Laser, which is financed by the Netherlands Organisation for Scientific Research (NWO).

[1] M. Anderson, J. Ensher, M. Matthews, C. Wieman, and E. Cornell, Science **269**, 198 (1995).
[2] M. O. Mewes, M. R. Andrews, N. J. Vandruten, D. M. Kurn, D. S. Durfee, and W. Ketterle, Phys. Rev. Lett. **77**, 416 (1996).
[3] C. C. Bradley, C. A. Sackett, and R. G. Hulet, Phys. Rev. Lett. **78**, 985 (1997).
[4] H. Metcalf and P. van der Straten, *Laser Cooling and Trapping* (Springer-Verlag, New York, 1999).
[5] H. F. Hess, Phys. Rev. B **34**, 3476 (1986).
[6] N. Masuhara, J. M. Doyle, J. C. Sandberg, D. Kleppner, T. J. Greytak, H. F. Hess, and G. P. Kochanski, Phys. Rev. Lett. **61**, 935 (1988).
[7] W. Ketterle and N. van Druten, Adv. Atom. Mol. Opt. Phys. **37**, 181 (1996).
[8] K. Davis, M. Mewes, and W. Ketterle, App. Phys. B **60**, 155 (1995).
[9] O. Luiten, M. Reynolds, and J. Walraven, Phys. Rev. A **53**, 381 (1996).
[10] M.-O. Mewes, M. R. Andrews, D. M. Kurn, D. S. Durfee, C. G. Townsend, and W. Ketterle, Phys. Rev. Lett. **78**, 582 (1997).
[11] B. P. Anderson and M. A. Kasevich, Science **282**, 1686 (1998).
[12] I. Bloch, T. W. Hänsch, and T. Esslinger, Phys. Rev. Lett. **82**, 3008 (1999).

[13] E. W. Hagley, L. Deng, M. Kozuma, J. Wen, K. Helmerson, S. L. Rolston, and W. D. Phillips, Science **283**, 1706 (1999).
[14] W. Ketterle, Rev. Mod. Phys. **74**, 1131 (2002).
[15] I. Bloch, M. Köhl, M. Greiner, T. W. Hänsch, and T. Esslinger, Phys. Rev. Lett. **87**, 030401 (2001).
[16] B. K. Teo and G. Raithel, Phys. Rev. A **63**, 031402 (2001).
[17] P. O. Schmidt, S. Hensler, J. Werner, T. Binhammer, A. Görlitz, and T. Pfau, J. Opt. B **5**, S170 (2003).
[18] T. Lahaye, J. M. Vogels, K. J. Guenter, Z. Wang, J. Dalibard, and D. Guéry-Odelin, Phys. Rev. Lett. **93**, 093003 (2004).
[19] T. Lahaye and D. Guéry-Odelin, Eur. Phys. J. D **33**, 67 (2005).
[20] T. Lahaye, Z. Wang, G. Reinaudi, S. P. Rath, J. Dalibard, and D. Guéry-Odelin, Phys. Rev. A **72**, 033411 (2005).
[21] T. Lahaye and D. Guéry-Odelin, Phys. Rev. A **73**, 063622 (2006).
[22] S. E. Olson, R. R. Mhaskar, and G. Raithel, Phys. Rev. A **73**, 033622 (2006).
[23] J.-F. Riou, W. Guerin, Y. Le Coq, M. Fauquembergue, V. Josse, P. Bouyer, and A. Aspect, Phys. Rev. Lett. **96**, 070404 (2006).
[24] A. Aghajani-Talesh, M. Falkenau, V. V. Volchkov, L. E. Trafford, T. Pfau, and A. Griesmaier, New J. Phys. **12**, 065018 (2010).
[25] K. B. Davis, M.-O. Mewes, M. A. Joffe, M. R. Andrews, and W. Ketterle, Phys. Rev. Lett. **74**, 5202 (1995).
[26] T. W. Hijmans, O. J. Luiten, I. D. Setija, and J. T. M. Walraven, J. Opt. Soc. Am. B **6**, 2235 (1989).
[27] D. Pritchard, K. Helmerson, and A. Martin, in *Atomic Physics II*, edited by S. Haroche, J. Gay, and G. Grynberg (World Scientific, Singapore, 1989), p. 179.
[28] E. W. Streed, A. P. Chikkatur, T. L. Gustavson, M. Boyd, Y. Torii, D. Schneble, G. K. Campbell, D. E. Pritchard, and W. Ketterle, Rev. Sci. Instrum. **77**, 023106 (2006).
[29] E. Mandonnet, A. Minguzi, R. Dum, I. Carusotto, Y. Castin, and J. Dalibard, Eur. Phys. J. D **10**, 9 (2000).